Electronic Supplementary Information

Convergent paired electrosynthesis of dimethyl carbonate from carbon dioxide enabled by designing the superstructure of axial oxygen coordinated nickel single-atom catalyst

Xiaofang Li[a], Shu-Guo Han[a], Weiming Wu[a], Kexin Zhang[e], Bo Chen[f], Sheng-Hua Zhou[a], Dong-Dong Ma[a], Wenbo Wei[a], Xin-Tao Wu[a,b,c], Ruqiang Zou[d] & Qi-Long Zhu[a,b,c]*

[a] State Key Laboratory of Structural Chemistry, Fujian Institute of Research on the Structure of Matter, Chinese Academy of Sciences (CAS), Fuzhou 350002, China.

[b] Fujian Science & Technology Innovation Laboratory for Optoelectronic Information of China, Fuzhou 350108, China.

[c] University of Chinese Academy of Sciences, Beijing 100049, China.

[d] Beijing Key Laboratory for Theory and Technology of Advanced Battery Materials, School of Materials Science and Engineering, Peking University, Beijing 100871, China.

[e] China Huaneng Group Clean Energy Technology Research Institute Co., Ltd., Changping District, Beijing 102209, China.

[f] Department of Chemistry, City University of Hong Kong, Hong Kong, China.

Experimental Section

Materials: Styrene (99%) was obtained from Aladdin Co., and further washed by sodium hydroxide (NaOH, A.R., Sinopharm Chemical Reagent Co. (SCRC), 5 wt%) aqueous solution to remove the stabilizing agent (*p*-tert-butylcatechol). Potassium peroxodisulfate ($K_2S_2O_8$, A.R., SCRC) was recrystallized before use. Polyvinyl pyrrolidone (PVP, MW 55000, Aladdin Co.), Pluronic® F127 (bioreagent, Sigma), phenol (A.R., SCRC), formaldehyde solution (37 wt%, A.R., SCRC), nickel nitrate hexahydrate ($Ni(NO_3)_2 \cdot 6H_2O$, A.R., SCRC), iron nitrate nonahydrate ($Fe(NO_3)_2 \cdot 9H_2O$, A.R., SCRC), cobalt nitrate hexahydrate ($Co(NO_3)_2 \cdot 6H_2O$, A.R., SCRC), melamine ($C_3H_6N_6$, A.R., SCRC) were used as received without further purification.

Preparation of PS template: Monodisperse PS spheres were synthesized using a typical emulsion polymerization. Typically, ultrapure water (100 mL, 18 MΩ cm^{-2} @ 25 °C), PVP (0.5 g) and styrene (13 mL) were added into a three-necked, round-bottomed flask (250 mL). The mixture was stirred at 500 rpm, while being heated to 70 °C and purged with nitrogen gas with a flow rate of 80 mL min^{-1}. After the mixture was kept at 70 °C for 20 min, $K_2S_2O_8$ solution (20 mL, 1.5 wt%) was added and the reaction was lasted for 24 h. The resulting PS spheres were centrifuged at 4000 rpm to remove any large agglomerates in the bottom. Then the colloidal PS solution in the upper was centrifuged, washed with ethanol and dried at 60 °C overnight to obtain the ordered PS template.

Preparation of resol: Typically, phenol (10 g) was melted at 42 °C and then NaOH solution (2.1 g, 20 wt%) was added dropwise with continuous stirring at 100 rpm. After the formaldehyde solution (17.7 g, 37 wt%) was added, the solution was kept at 70 °C for another 1 h and then cooled down to room temperature. The pH value of the obtained solution was adjusted to 7 with aqueous HCl solution (2 M). Then, water was removed by rotary evaporation and the product was diluted into a resol solution (20 wt%) with ethanol. During the dilution, the separated NaCl was filtered to obtain a pale-yellow solution.

Preparation of Ni SAs/OMMNC: F127 (0.6 g) and $Ni(NO_3)_2 \cdot 6H_2O$ (0.1 g) were dissolved in the obtained resol solution (5 g) under ultrasonication for 30 min to obtain a green precursor solution. Then, a forced impregnation method was used to infiltrate the voids between the ordered PS templates. Typically, the ordered PS template (1.0 g) was immersed into the precursor solution for 1 hour and further treated with vacuum degassing for 10 min to make all voids between PS spheres fully filled with precursor solution. After keeping still under room temperature for 12 h, the excess solution was removed by filtration. The obtained composite was heated at 100 °C in air for 24 h and then at 350 °C for 2 h with a ramp rate of 2 °C min^{-1} under Ar gas flowing, followed by washing in acetone and cyclohexane mixture (1:1 of v/v) at 60 °C under continuous stirring to remove the residual template. The solid was filtered and dried at 60 °C overnight. Then the obtained solid was mixed with 10 times weight of melamine and pyrolyzed at 550 °C for 2 h with a ramp rate of 2 °C min^{-1} and then 900 °C for 2 h with a ramp rate of 5 °C min^{-1} under Ar gas flowing. Finally, Ni SAs/OMMNC was produced by acid etching with aqueous HCl solution (2 M) for 24 h. For comparison, Ni SAs/OMNC and OMMNC were also prepared by following the same procedure without adding F127 and $Ni(NO_3)_2 \cdot 6H_2O$ in the precursors, respectively. Ni NPs/OMMC was synthesized without adding melamine in the pyrolysis process. OMMC was obtained without adding $Ni(NO_3)_2 \cdot 6H_2O$ and melamine in the precursors in the pyrolysis process.

Characterization: The SEM images of the obtained samples were observed by a field-emission scanning electron microscopy (FESEM, JSM6700, operated at an accelerating voltage of 5 kV). The TEM images, HAADF-STEM images and elemental mapping were recorded on transmission electron microscopy (TEM, F20, operated at an accelerating voltage of 200 kV). The PXRD patterns of the samples were measured by a Miniflex600 X-ray diffractometer at 40 kV and 40 mA with Cu K_α radiation. The N_2 sorption of the samples was measured on a BELSORP Max analyzer at 77 K. The XPS spectroscopy with monochromatized Al K_α X-rays (hv = 1486.6 eV) radiation (ThermoFisher Scientific Co. ESCALAB 250Xi, USA) was used to

investigate the surface electronic properties. The BE calibration of the spectra was referred to the C 1s peak located at BE = 284.8 eV for the analysis.

Electrochemical CO₂RR measurement: The electrochemical CO$_2$RR was performed in an H-type cell with Nafion 117 membrane between the cathodic chamber and anodic chamber. 0.5 M KHCO$_3$ was used as the electrolyte throughout the whole measurements. The electrochemical measurements were performed at a CHI660E electrochemical workstation (CH Instruments, USA), in which Pt mesh and Ag/AgCl was used as the counter and reference electrodes, respectively. All the potentials were calibrated to the RHE using the following equation: $E_{RHE} = E_{Ag/AgCl} + 0.1989$ V $+ 0.059$ pH (the pH of CO$_2$-saturated KHCO$_3$ was 7.2). The catalyst ink was prepared by mixing H$_2$O (0.35 mL), EtOH (0.1 mL), Nafion solution (0.05 mL, 5 wt% in isopropanol) and catalyst (5.0 mg) together, followed by ultrasonication for 1 h. Then, the ink (25 μL) was uniformly loaded onto the both sides of the hydrophobic CP with 1 × 1 cm^2, resulting in a catalyst loading of 0.5 mg cm^{-2}. Before electrochemical CO$_2$ reduction, high-purity CO$_2$ gas was bubbled through the solution for at least 10 min. A mass flow controller was used to set the CO$_2$ flow rate at 20 sccm. After that, the electrochemical accessibility of the working electrode was optimized by potential cycling between −0.30 and −1.07 V *vs* RHE at a scan rate of 50 mV s^{-1} until stable voltammogram curves were obtained. Then, the polarization curves were recorded at a scan rate of 10 mV s^{-1}. The chronoamperometry or chronopotentiometry tests were conducted at each potential or current density for 60 min. All the potentials and currents were reported as measured without *iR* and current correction in H-type cell.

The electrochemical CO$_2$RR in a Teflon four-part flow cell is consisted of a gas-duffusion layer (CeTech GDL 340) as the cathode, an anion exchange membrane, a NiFe layered double hydroxide (LDH) supported on Ni foam (2.0×2.0 cm^2) as the anode and an Ag/AgCl electrode. The catalyst ink was uniformly loaded onto the GDL with 1 × 1 cm^2, resulting in a catalyst loading of 1 mg cm^{-2}. The cathode and anode are connected with copper tape and Ti mesh,

respectively. 1.0 M KOH was used as the electrolyte throughout the measurements. Prior to the test, the electrolyte was circulated in the cathode and anode chambers by using peristaltic pumps. All the potentials were reported with 90%-iR correction in flow cell.

The gas products of electrolysis were continuously plunged into the gas sampling loop (250 µL) of Agilent 7820A gas chromatography equipped with TCD detector, FID detector and molsieve 5A packed column. High purity argon (99.9999%) was used as the carrier gas for the gas chromatography. The quantification for each gas was determined by external standard method. Liquid products were analyzed by quantitative NMR using dimethyl sulphoxide as an internal standard after CO_2 reduction electrolysis for 60 min (500 µL electrolyte was mixed with 100 µL D_2O ($KHCO_3$ electrolyte)/DMSO-D6 (KBr-CH_3OH electrolyte) containing 0.1 µL DMSO). Solvent presaturation technique was implemented to suppress the solvent peak. ^1H NMR spectra were recorded on an ECZ400S 400 MHz spectrometer.

The FE of CO was calculated by the equation:

$$FE_{CO} = \frac{J_{co}}{J_{total}} = \frac{v_{co} \times N \times F}{J_{total}}$$

$J_{CO:}$ partial current density for CO production, A;

$J_{total:}$ total current density, A;

$N:$ the number of the electron transferred for forming a product molecule, which is 2 for CO;

$v_{co}:$ the product rate of CO, which was calculated based on the equation of $v_{co} = \dfrac{V_{co} \times v_{co2}}{V_m}$,

using the volume concentration of CO (V_{co}) measured by GC, the CO_2 flow rate (v_{co2}) and the molar volume of gas (V_m);

$F:$ Faradaic constant, 96485 C mol^{-1}.

The TOF value of the electrocatalyst was calculated by the equation:

$$TOF = \frac{J_{product}/NF}{m_{cat} \times \omega/M_{Ni}} \times 3600$$

$TOF:$ turnover frequency, h^{-1}

m_{cat}: catalyst mass in the electrode, g;

ω: Ni loading in the catalyst;

M_{Ni}: atomic mass of Ni, 58.69 g/mol.

The double-layer capacitance measurements were performed between −0.177 and −0.277 V *vs* RHE with an increasing scan rate of 5 mV in H-type cell. The impedance spectra were recorded at −0.77 V *vs* RHE in the frequency range from 10^5 to 0.01 Hz with a 10 mV peak-to-peak sinusoidal potential perturbation in H-type cell.

The convergent paired electrosynthesis of DMC from CO$_2$: The electrochemical CO$_2$RR measurement in 0.1 M KBr-CH$_3$OH in an H-type cell was similar to that in 0.5 M KHCO$_3$, except that the potential calibration was not used. The convergent paired electrosynthesis of DMC was performed in a membrane-free single cell, where a two-electrode system with Ni SAs/OMMNC as the cathode and CC as the anode was used. A CO$_2$-saturated 0.1 M KBr-methanol solution was used as the electrolyte where Pd/C (40 mg) catalyst was homogeneously dispersed. During bulk electrolysis, the cell was tightly sealed and the total charge passed was 30 C. After electrolysis, the solution was filtered and further analyzed on the Agilent 6820A gas chromatography equipped with FID detector and HP-5 column. The FE of DMC were calculated by using the following equations:

$$FE_{DMC} = \frac{2F \times n_{DMC}}{Q}$$

n_{DMC}: the moles of DMC, mol;

Q: the total charge passed, C.

The DFT calculation: First-principle calculations were performed with use of the Vienna Ab initio Simulation Package (VASP), by which the geometric structures of all systems were relaxed and the energies were obtained correspondingly. The interaction between the electrons and ions was characterized by the method of projector augmented wave (PAW). Electronic exchange and correlation interactions were described by the functional of generalized gradient

6

approximation (GGA). The planewave basis set along with a kinetic cutoff energy was 400 eV. The Monkhorst–Pack meshes of Brillouin zone was $3 \times 3 \times 1$. The force and energy criteria on each atom were -0.02 eV Å^{-1} and 10^{-5} eV, respectively. The O-Ni-N$_4$-C, Ni-N$_4$-C, N-C and Ni(111) surface were modeled by supercells. A vacuum layer of at least 20 Å was added to eliminate the interactions of two neighboring supercells along the z-axis. The van der Waals interaction was considered using the DFT-D3 scheme.

The adsorption energy was defined as:

$$E_{ads} = E_{cat+m} - E_{cat} - E_m$$

where E_{cat+m}, E_{cat} and E_m denote the total energies of the adsorbed system, the catalyst, and the adsorbate at free state, respectively, each of which can be obtained directly from DFT calculations.

The Gibbs free energy of each species was calculated as follows:

$$\Delta G = \Delta E + \Delta E_{ZPE} - T\Delta S$$

ΔE is the reaction energy from the density functional theory calculations. ΔE_{ZPE} and ΔS are the zero point energy difference and the entropy difference between the products and the reactants at room temperature, respectively.
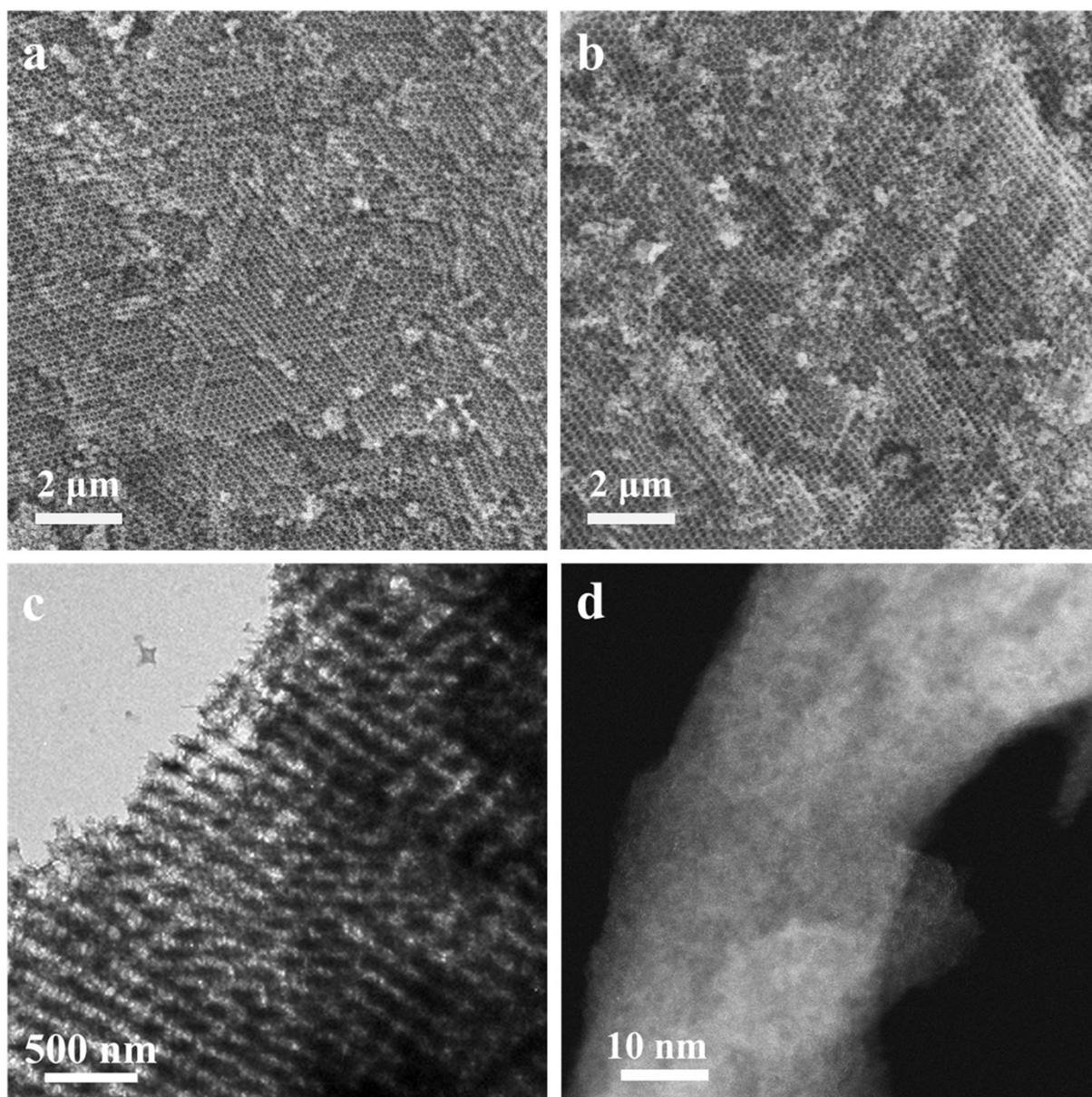
Fig. S1 SEM images of Ni SAs/OMMNC with the independent (a) 2nd and (b) 3rd preparation. (c) TEM image and (d) AC HAADF-STEM image of Ni SAs/OMMNC.
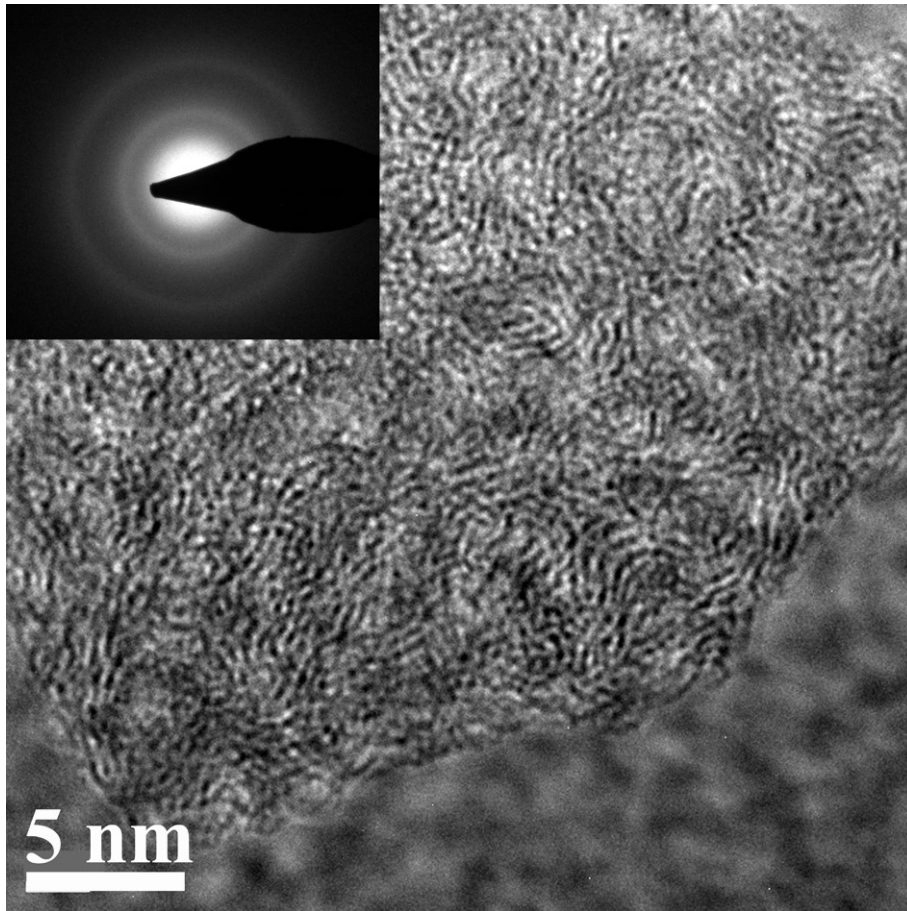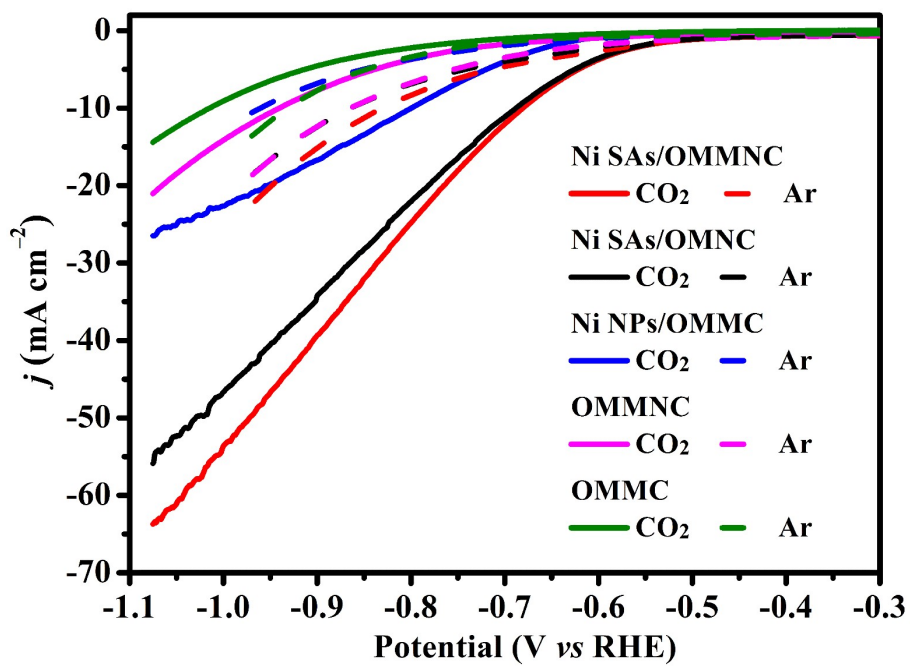
Fig. S2 High-resolution TEM image of Ni SAs/OMMNC.
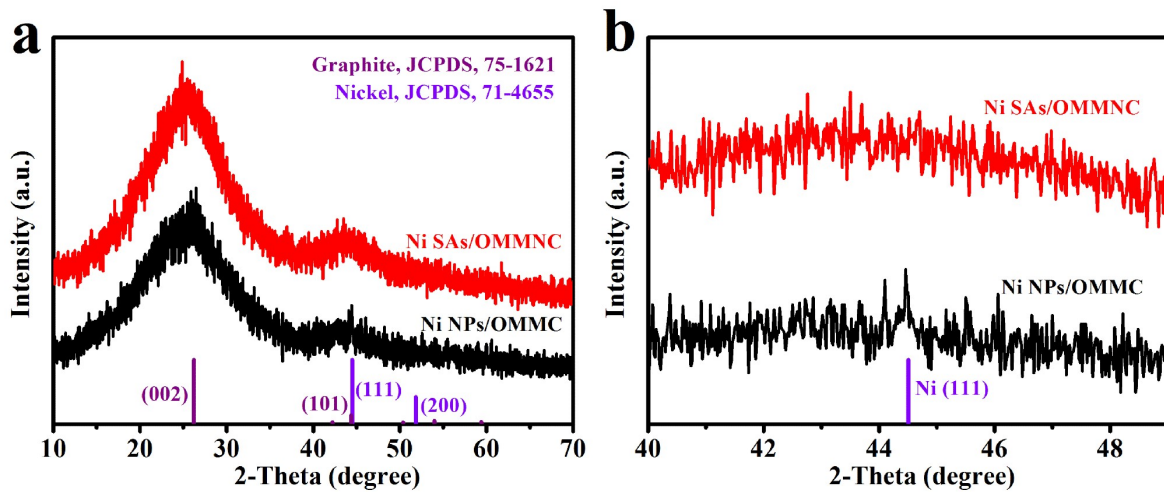
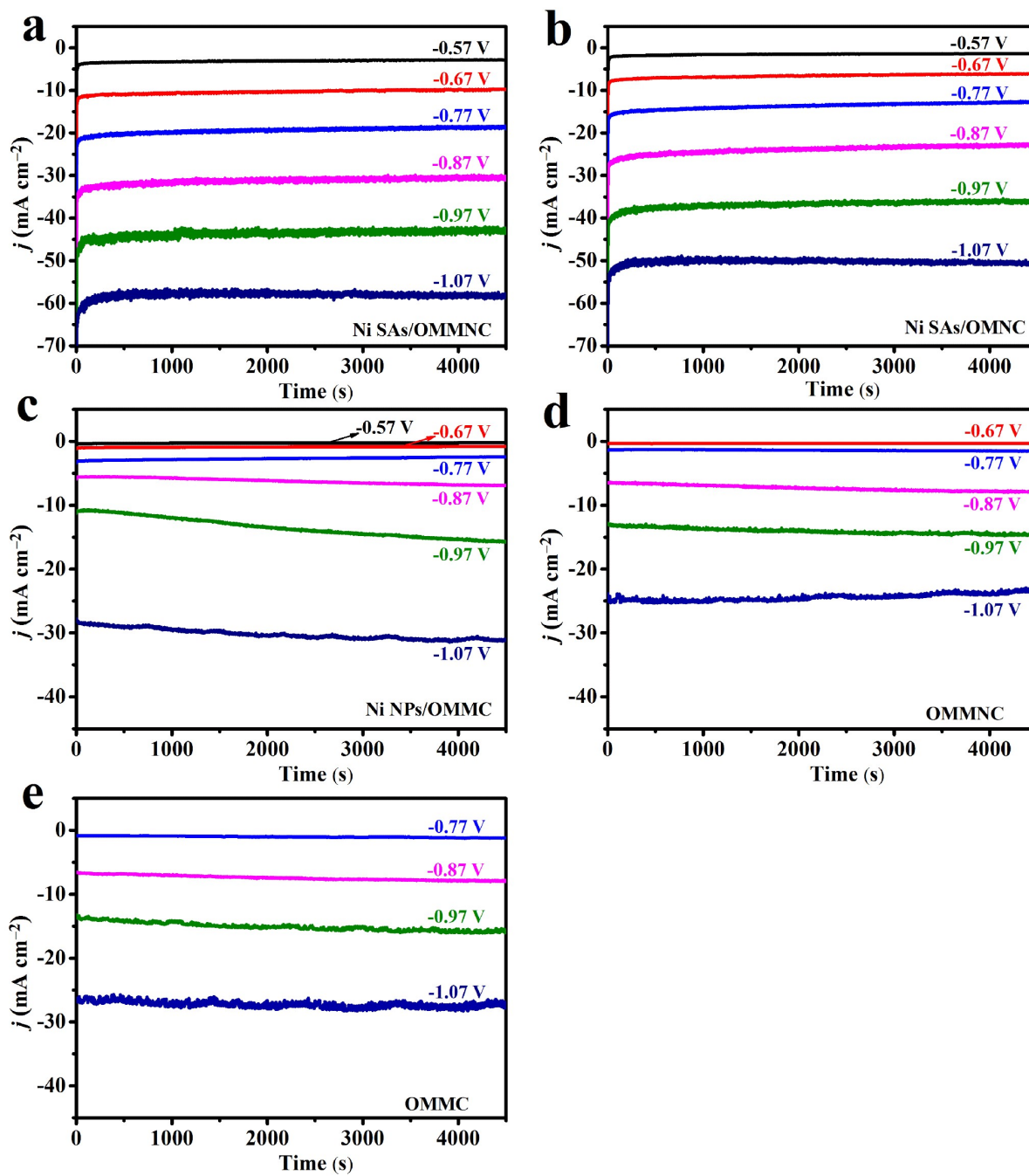**Fig. S3** (a) PXRD spectra and (b) the magnified PXRD spectra of Ni SAs/OMMNC and Ni NPs/OMMC.
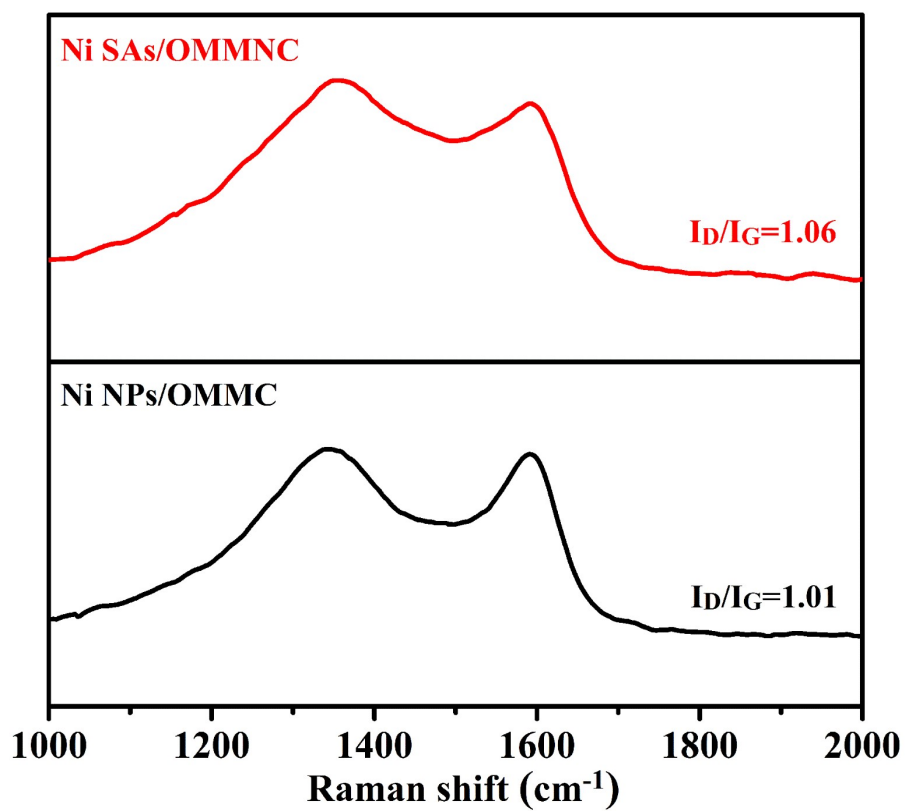
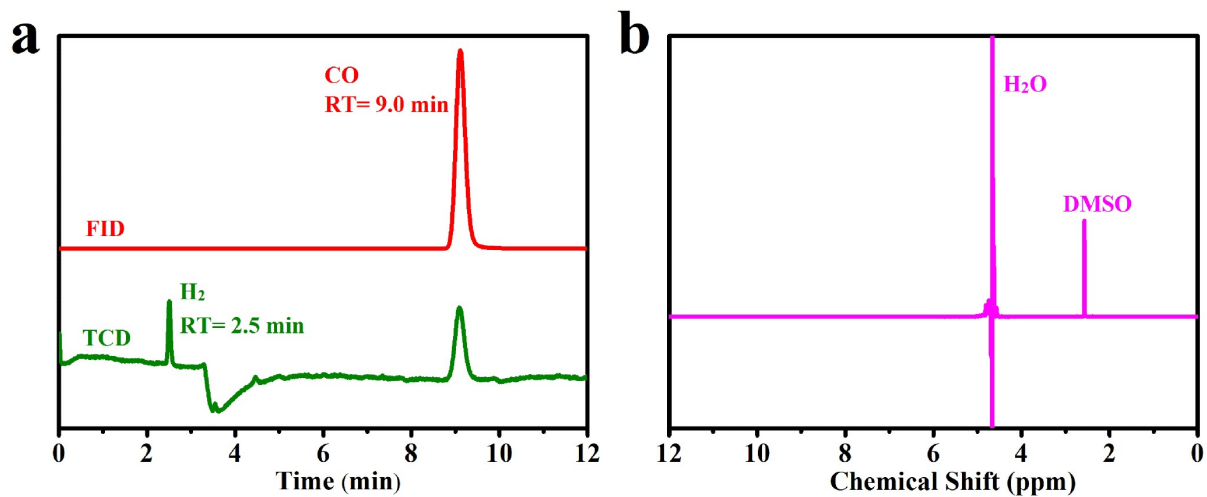**Fig. S4** Raman spectra of Ni SAs/OMMNC and Ni NPs/OMMC.
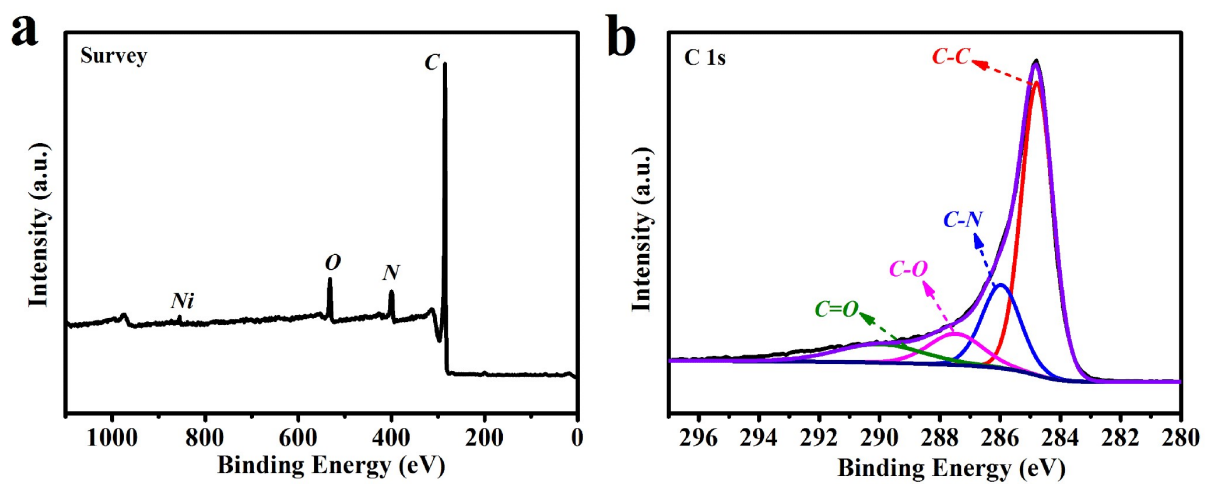
**Fig. S5** XPS (a) survey and (b) high-resolution C 1s spectra of Ni SAs/OMMNC.

Fig. S6 LSV of Ni SAs/OMMNC and the comparative samples in CO_2-saturated (solid lines) and Ar-saturated (dotted lines) 0.5 M $KHCO_3$.

Fig. S7 Bulk electrolysis of Ni SAs/OMMNC and compared samples at different applied potentials for electrocatalytic CO_2RR.

Fig. S8 (a) GC chromatogram and (b) NMR spectroscopy in D_2O of 0.5 M $KHCO_3$ electrolyte after the electrocatalytic CO_2RR.
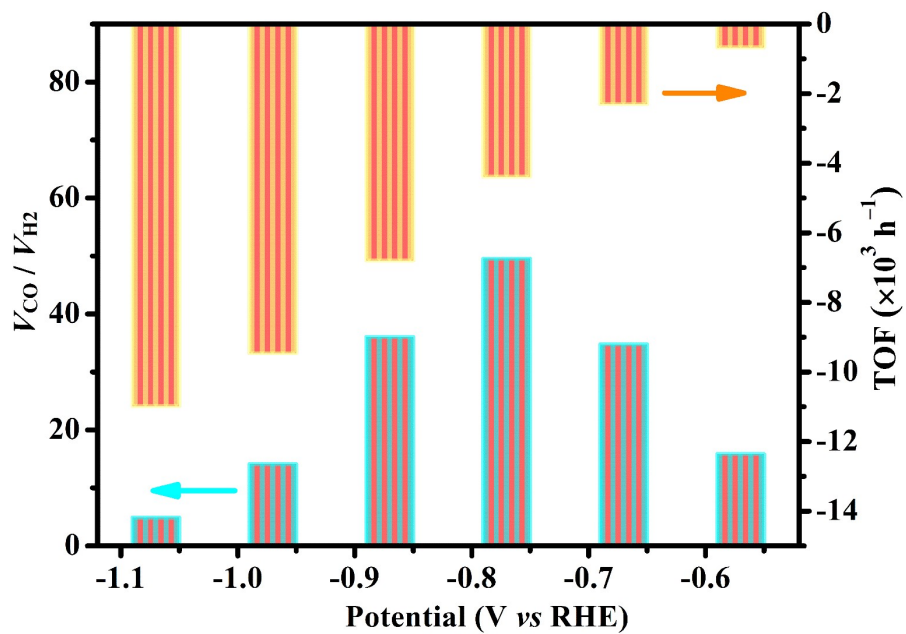
**Fig. S9** TOFs and volume CO/H$_2$ ratio of Ni SAs/OMMNC at different applied potentials.
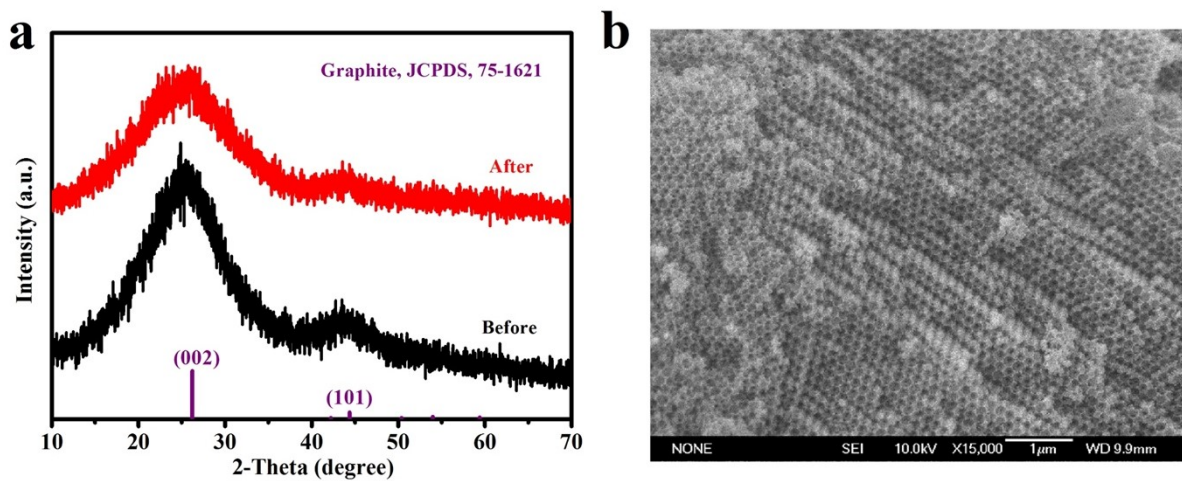
Fig. S10 (a) PXRD spectrum and (b) SEM image of Ni SAs/OMMNC after the long-term stability measurement in the H-type cell.
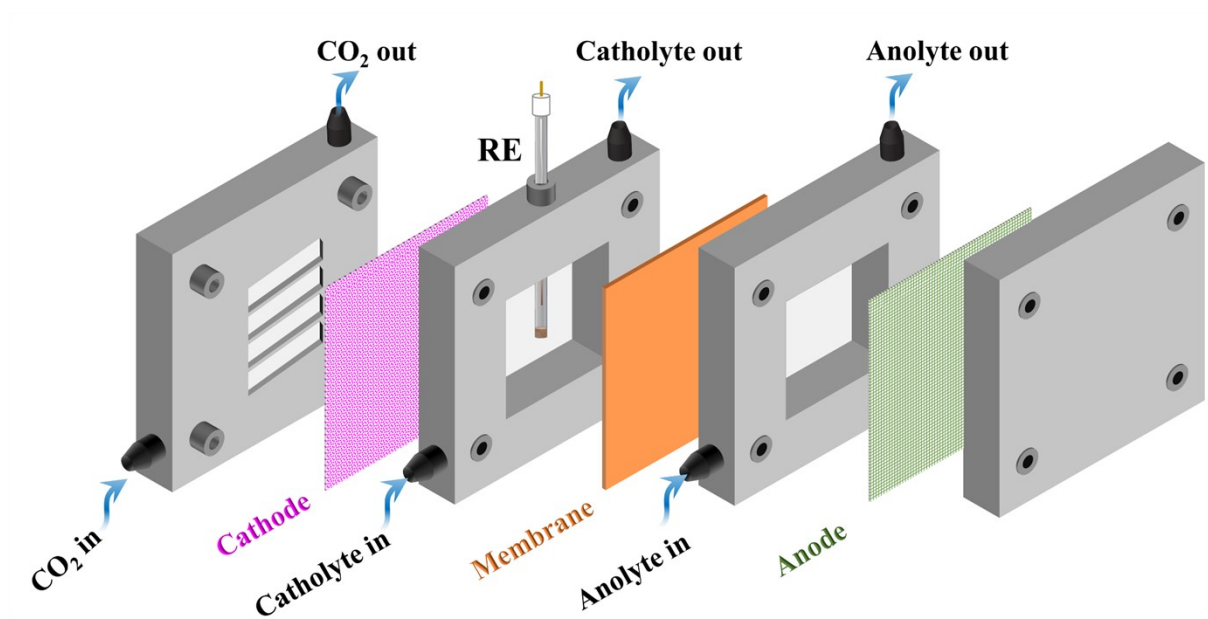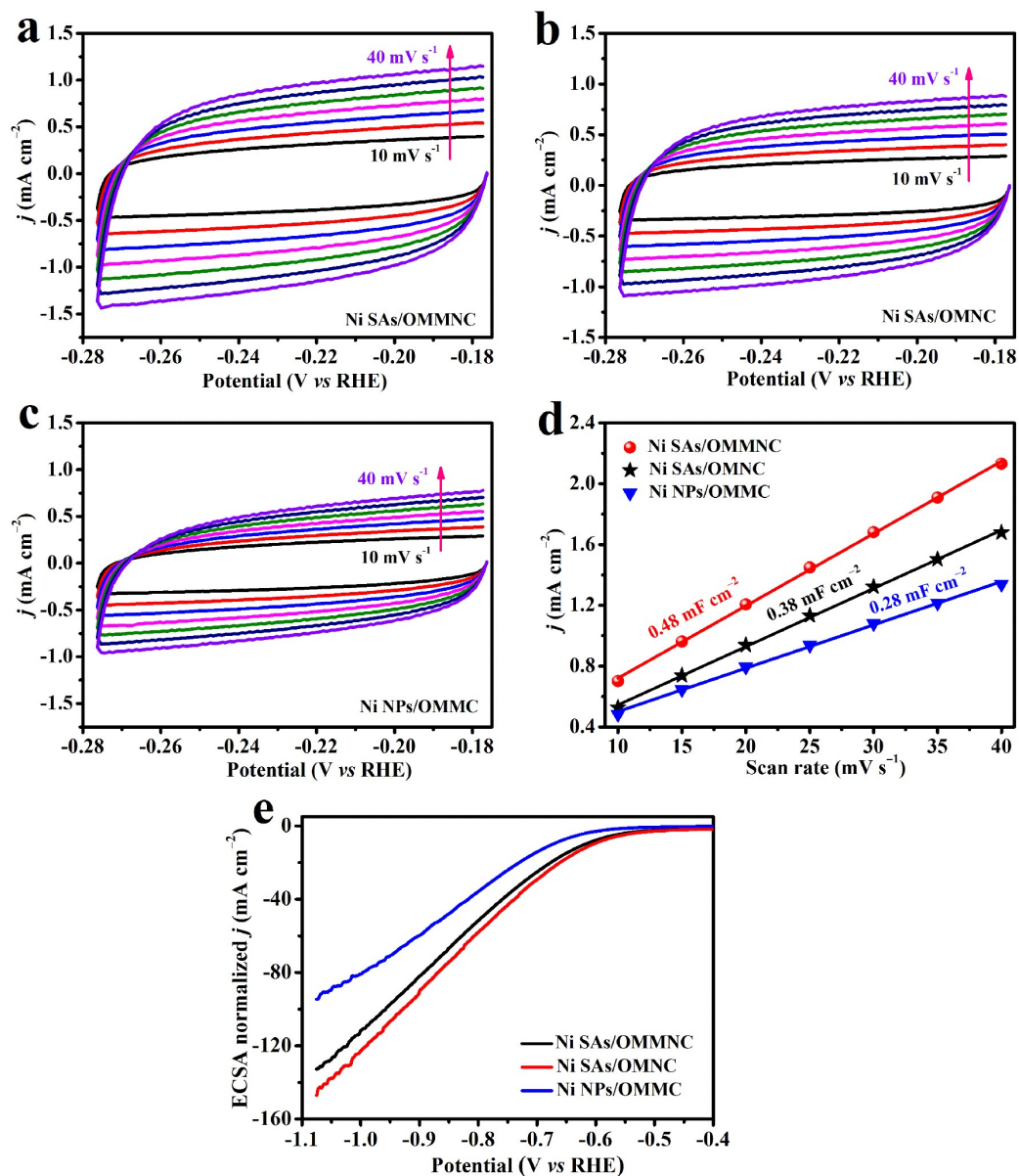
Fig. S11 Flow cell configuration for electrocatalytic CO$_2$RR.
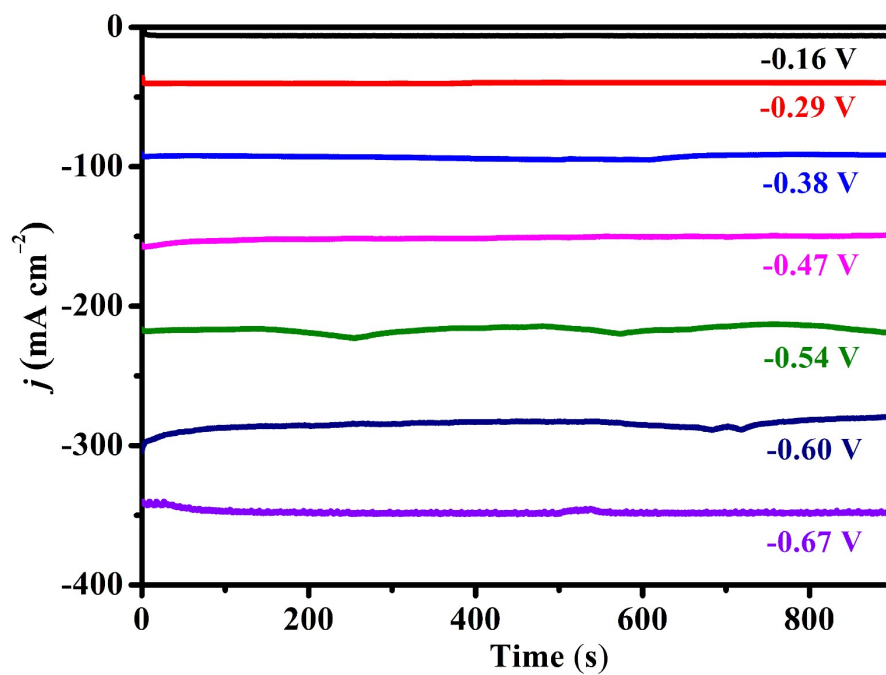
Fig. S12 Bulk electrolysis of Ni SAs/OMMNC in the flow cell at different applied potentials in 1 M KOH electrolyte.
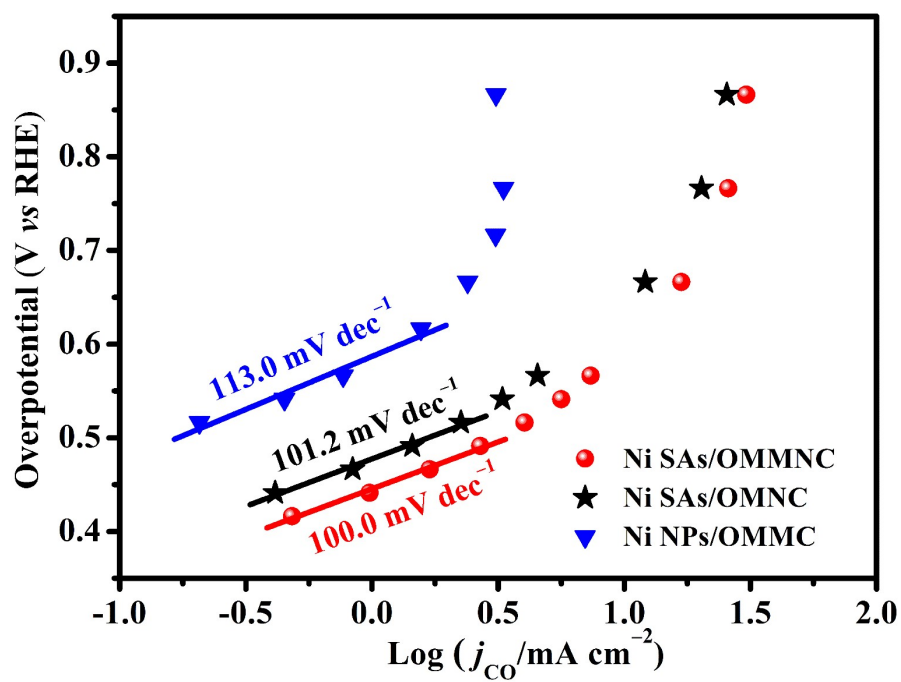
Fig. S13 The Tafel plots of Ni SAs/OMMNC and the comparative samples in CO_2-saturated 0.5 M $KHCO_3$ electrolyte.

Fig. S14 (a-c) Current density difference *vs* scan rate, (d) the corresponding yielded C_{dl} and (e) the ECSA normalized LSV plots of of Ni SAs/OMMNC and the comparative samples.
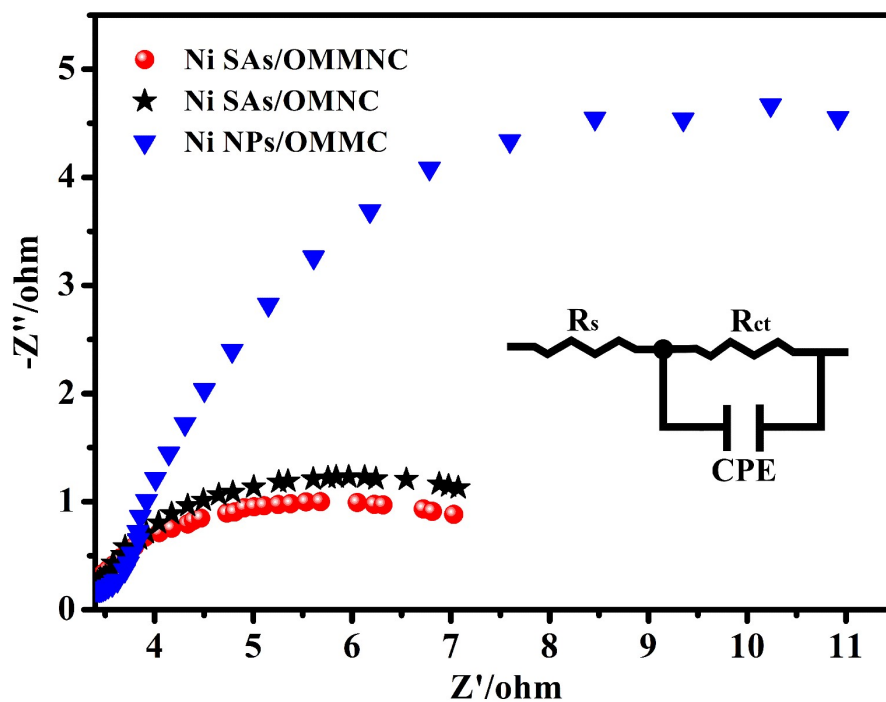
Fig. S15 EIS plots of Ni SAs/OMMNC and the comparative samples. Inset is the equivalent circuit consisting of an ohmic resistance of the electrolyte (R_s), a charge transfer resistance between catalyst and electrolyte (R_{ct}) and a constant phase element (CPE).
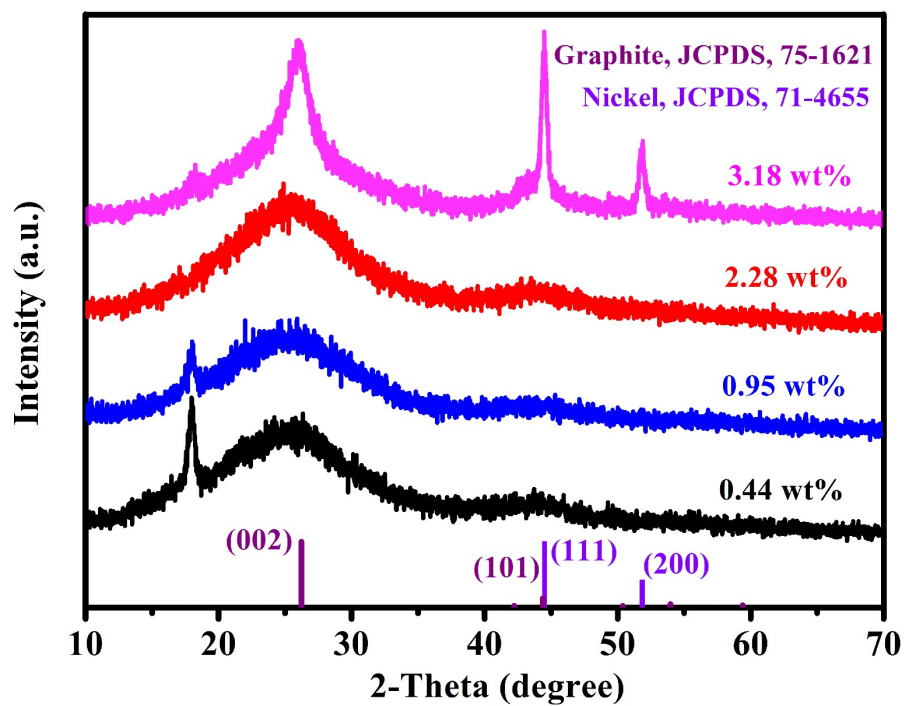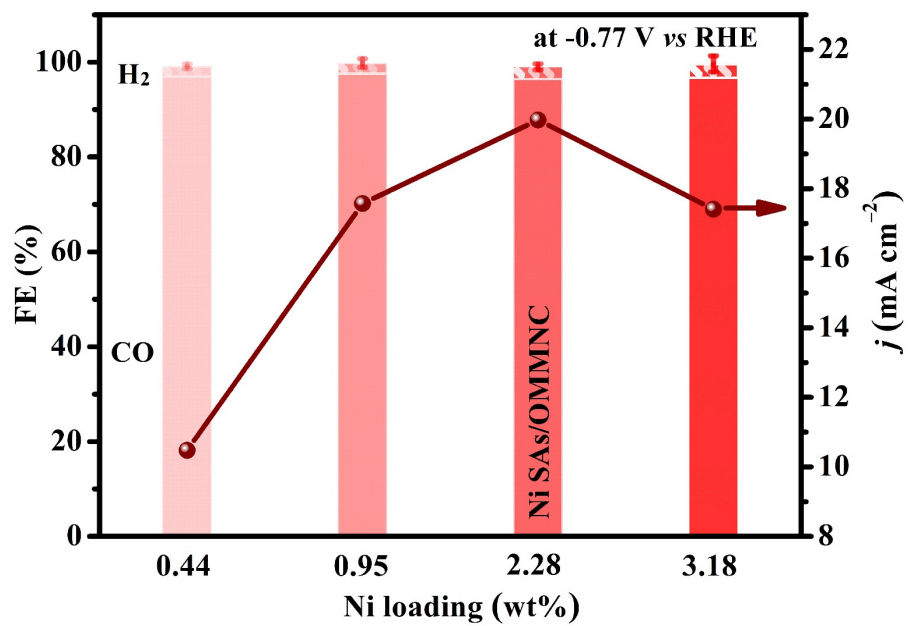
Fig. S16 PXRD spectra of Ni SAs/OMMNC and similarly constructed samples containing different Ni loadings.
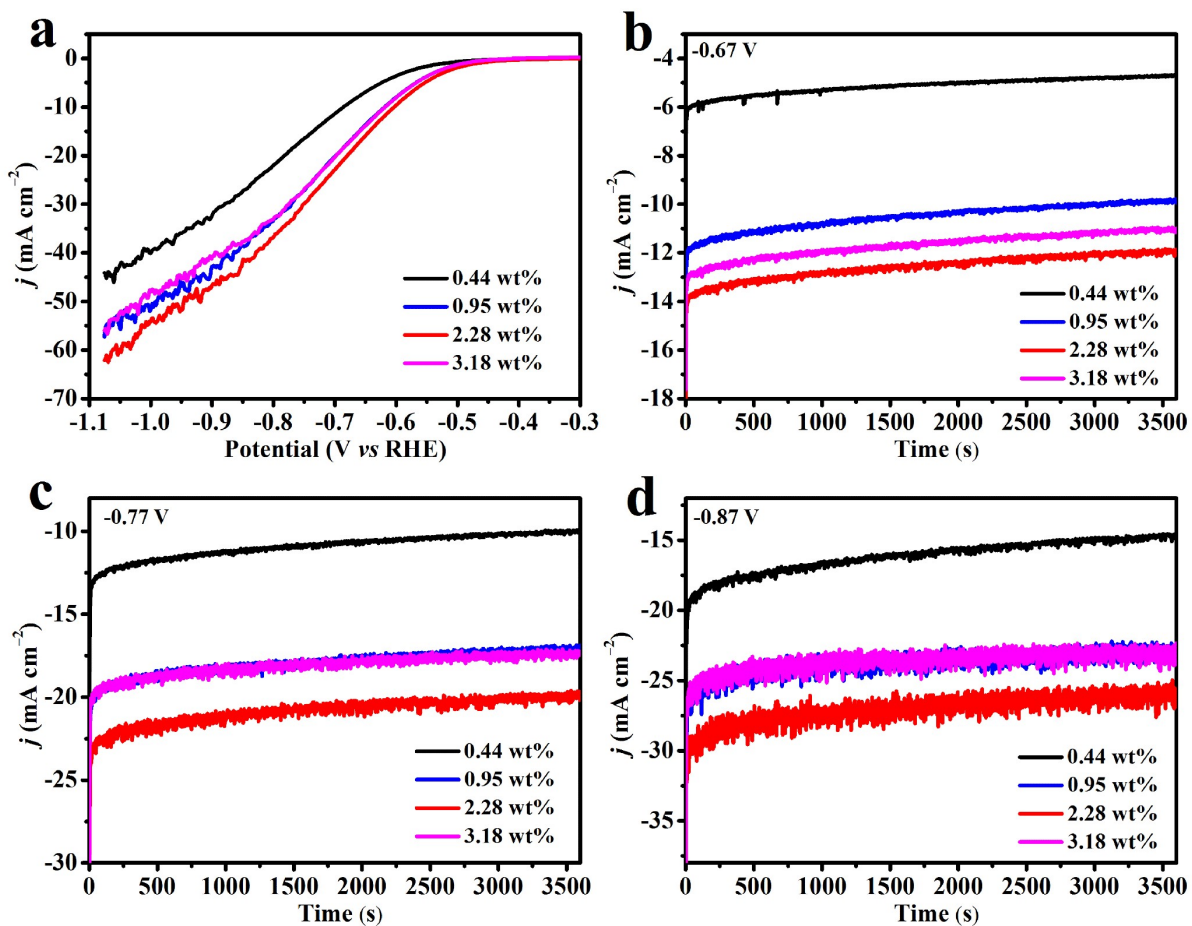
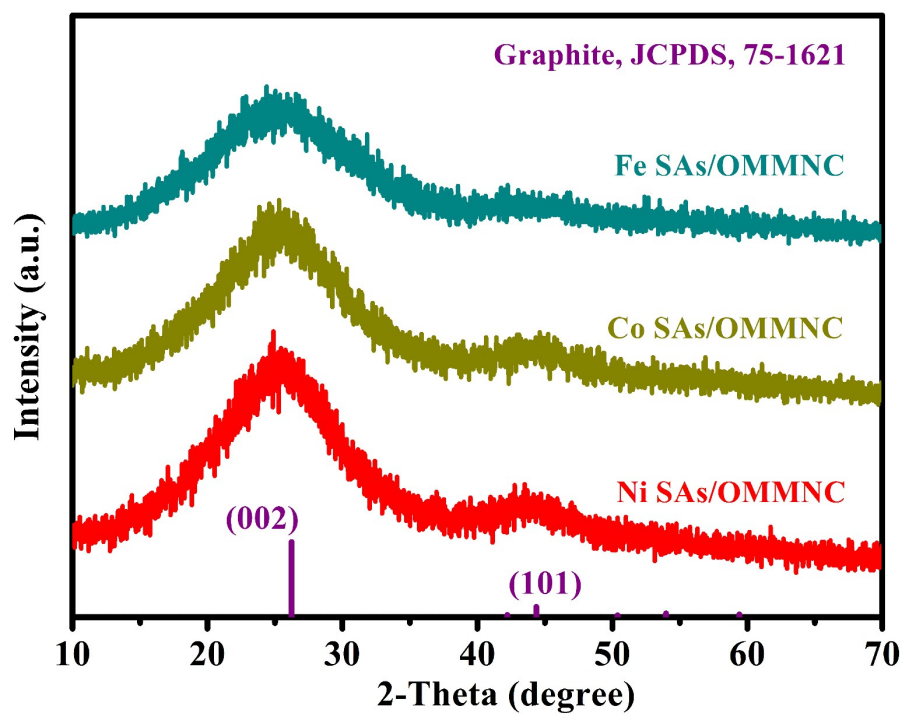**Fig. S17** LSV plots and bulk electrolysis of Ni SAs/OMMNC and similarly constructed samples containing different Ni loadings for electrocatalytic CO_2RR.
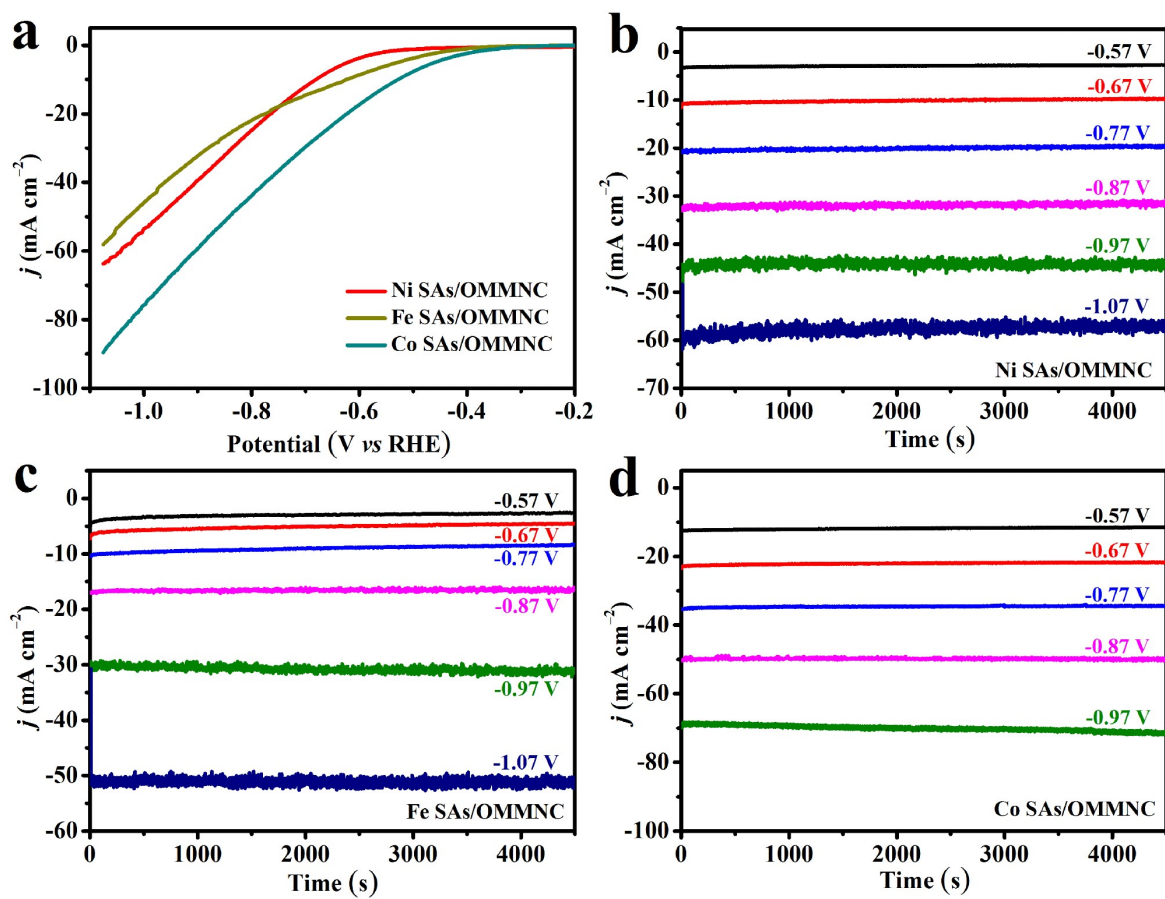
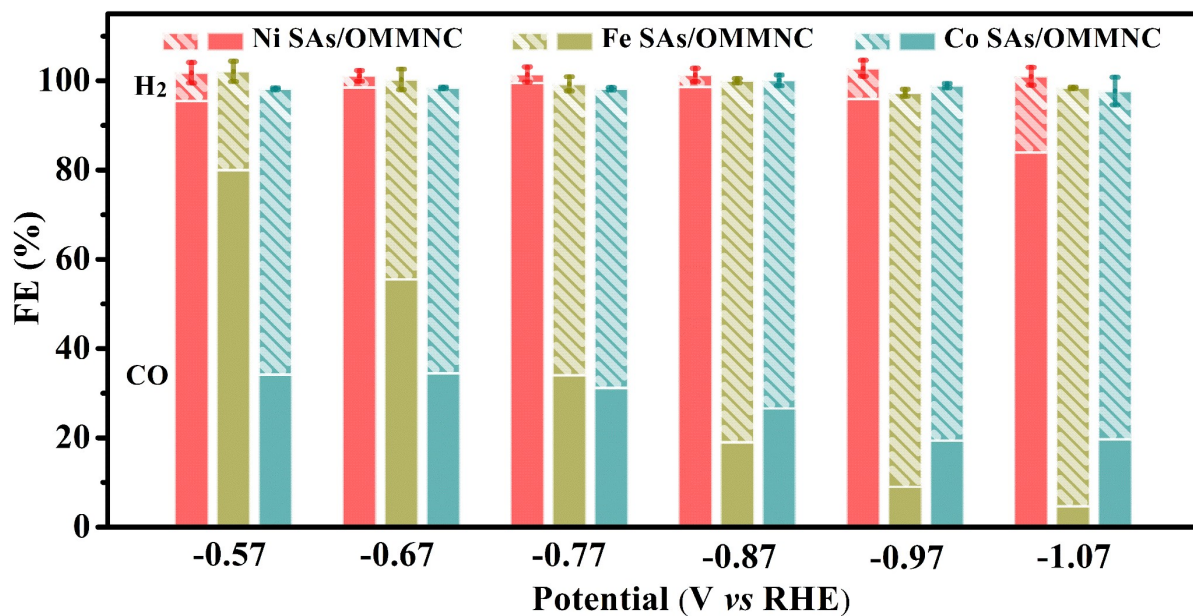**Fig. S18** Comparison of Ni SAs/OMMNC with similarly constructed samples containing different Ni loadings.

Fig. S19 PXRD spectra of X SAs/OMMNC (X=Fe, Co, Ni).

Fig. S20 (a) LSV plots and bulk electrolysis of (b) Ni SAs/OMMNC, (c) Fe SAs/OMMNC and (d) Co SAs/OMMNC for electrocatalytic CO_2RR.

Fig. S21 FE_{CO} and FE_{H_2} of Ni SAs/OMMNC, Fe SAs/OMMNC and Co SAs/OMMNC for electrocatalytic CO_2RR.
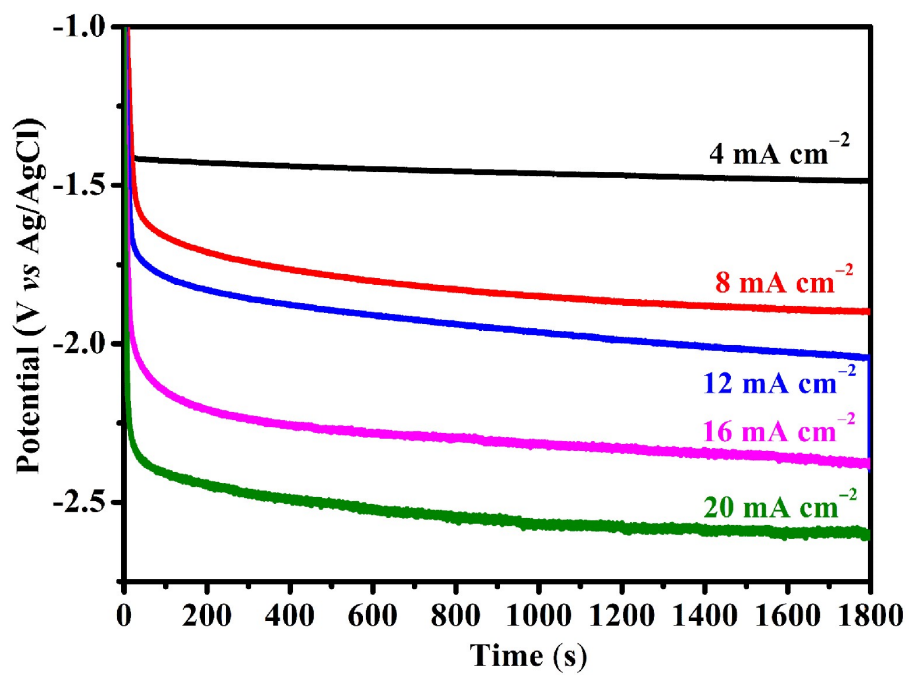
Fig. S22 Bulk electrolysis of Ni SAs/OMMNC at different current densities for electrocatalytic CO_2RR in 0.1 M KBr-CH_3OH solution in H-type cell.
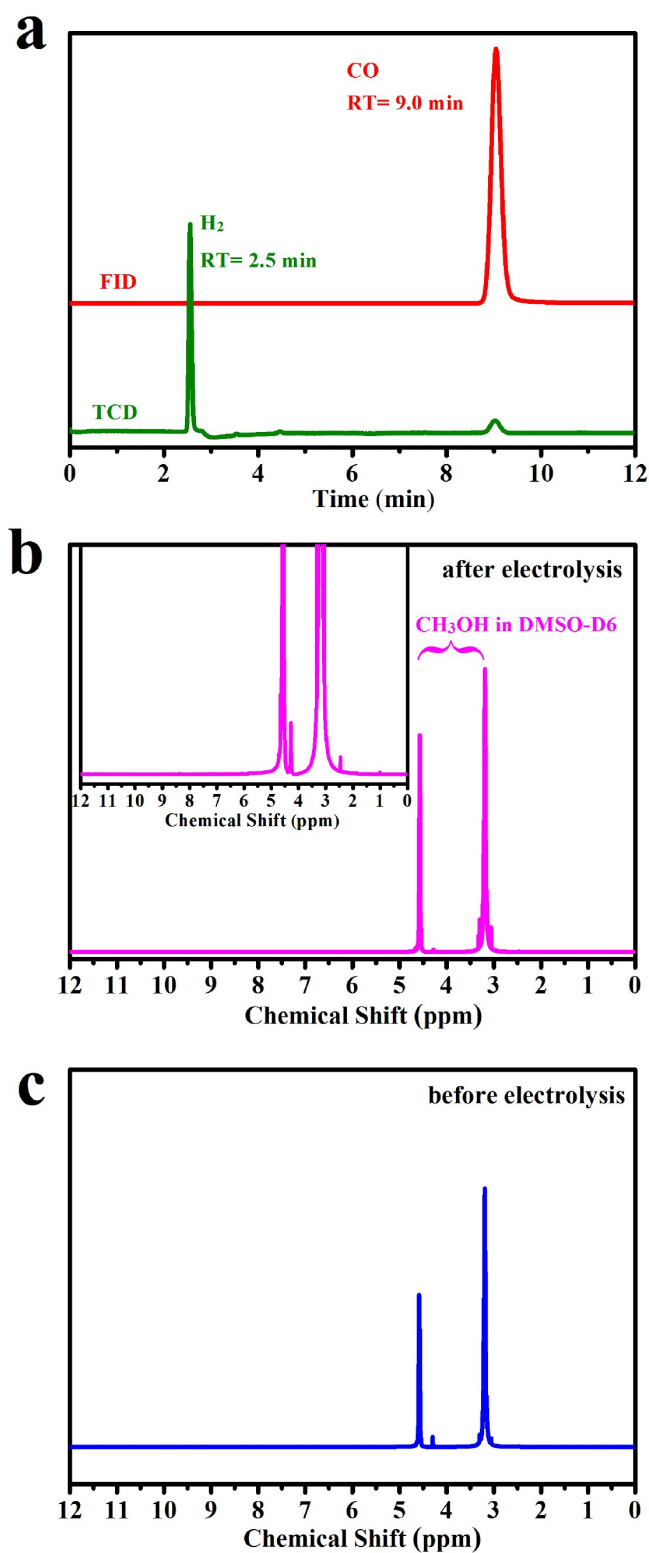
Fig. S23 (a) GC chromatogram, NMR spectroscopy in DMSO-d6 of 0.1 M KBr-CH$_3$OH electrolyte (b) after and (c) before the electrocatalytic CO$_2$RR.
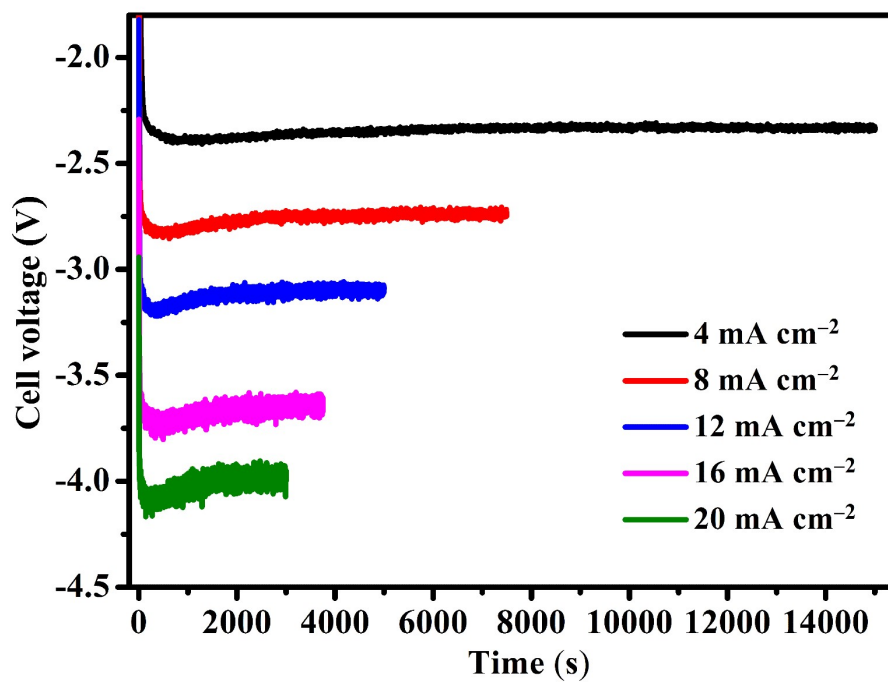
Fig. S24 Bulk electrolysis at different current densities for DMC electrosynthesis in 0.1 M KBr-CH$_3$OH solution in single cell. Total 30 C charge was passed for each electrolysis.
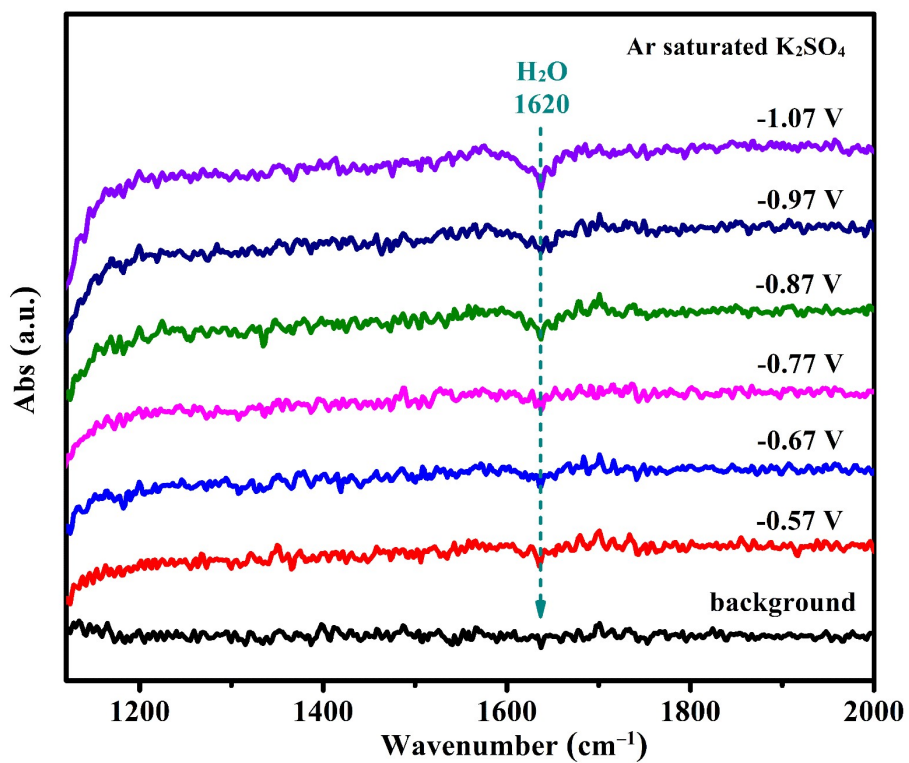
Fig. S25 *In situ* ATR-IR spectra of Ni SAs/OMMNC recorded at different applied potentials in Ar-saturated 0.5 M K_2SO_4 solution.
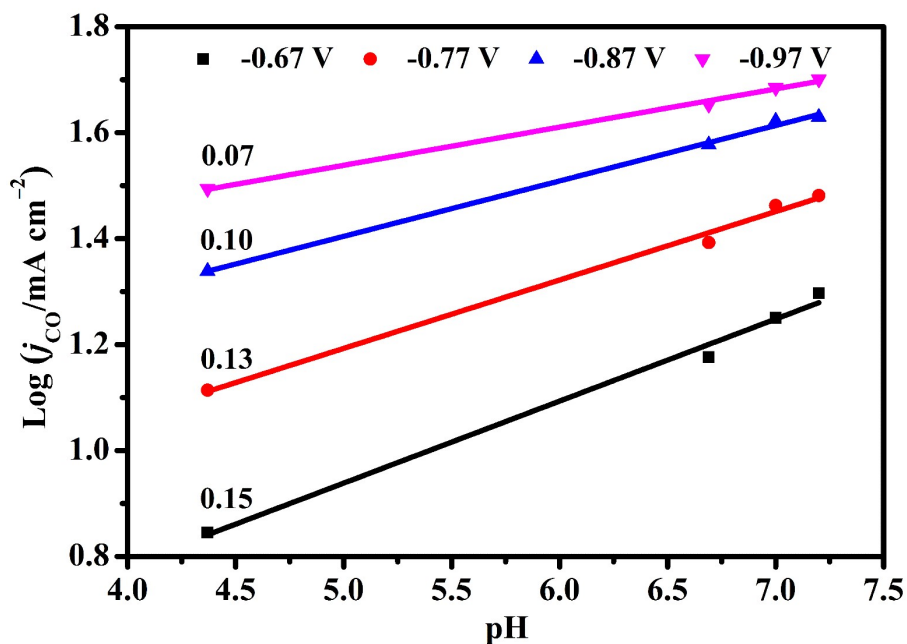
Fig. S26 pH dependence of j_{CO} at fixed potentials of Ni SAs/OMMNC.

Note:

For HCO_3^- dependence experiment, $KHCO_3$ and $KClO_4$ were used to make the electrolyte and the concentration of K^+ kept at 0.5 M. The data showed that j_{CO} of Ni SAs/OMMNC had an order of close to 0 in the concentration of HCO_3^-.

For pH dependence experiment, 0.5 M $KHCO_3$ solution (pH = 7.25), 0.17 M K_3PO_4 solution (pH = 7.00), 0.25 M K_2HPO_4 solution (pH = 6.69) and 0.5 M KH_2PO_4 solution (pH = 4.37) were used as the electrolytes. The data show that the pH of electrolyte have effect on the rate of reaction, indicating the pH buffer role of HCO_3^-.
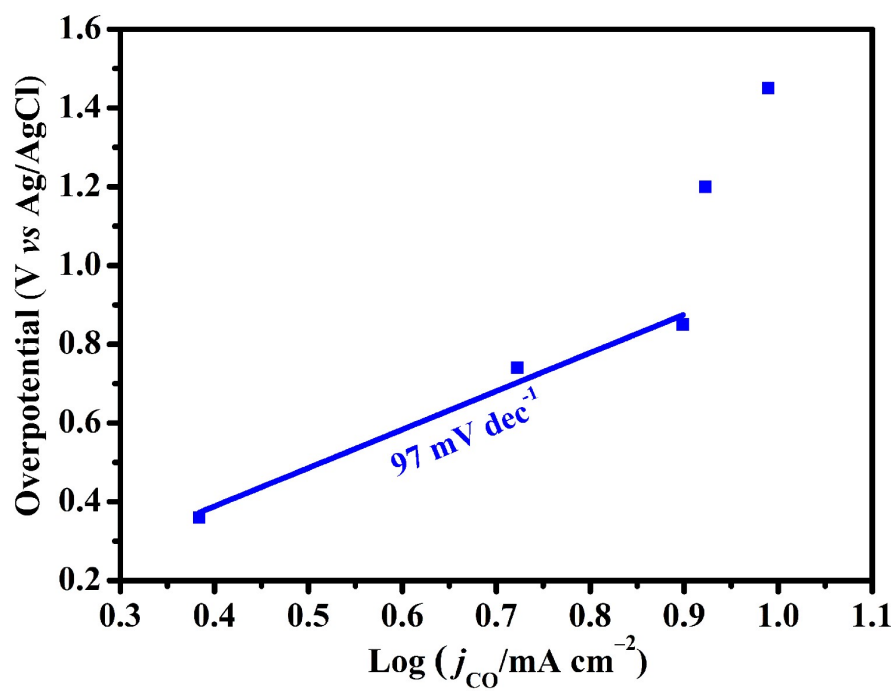
Fig. S27 The Tafel plots of Ni SAs/OMMNC and the comparative samples in CO_2-saturated 0.1 M KBr-CH_3OH electrolyte.

Table S1 Structural parameters of Ni SAs/OMMNC extracted from the Ni K-edge EXAFS fitting ($S_0^2 = 0.7$)

Samples	Path	N	R (Å)	$\sigma^2 \times 10^{-3}$ (Å)	ΔE_0 (eV)	R factor
Ni foil	Ni-Ni	12	2.484	4.7	6.66	0.01
NiO	Ni-O	6	2.080	2.9	-2.94	0.02
NiPc	Ni-N	4	1.871	3.3	-0.25	0.03
Ni SAs/OMMNC	Ni-N	4	1.953	2.7	-1.26	0.007
	Ni-O	1	2.115	5.7	-1.47	

Notes: S_0^2 is the amplitude reduction factor which was fixed as 0.7. N is the coordination number; R is interatomic distance (the bond length between central atom and surrounding coordination atom); σ^2 is Debye-Waller factor (a measure of thermal and static disorder in absorber-scatterer distances); ΔE_0 is the inner potential correction; R factor is used to value the goodness of fitting.

Table S2 Comparison of the catalytic performances of various electrocatalysts for CO_2RR in H-type cell.

Catalyst	Atomic configuration	Electrolyte	Ni loading	Potential (V *vs* RHE)	FE_{co}	j_{CO} (mA cm^{-2})	Ref
Ni SAs/ OMMNC	**O-Ni-N$_4$**	**0.5 M KHCO$_3$**	**2.28 wt%**	**−0.77** **−0.97**	**99%** **96%**	**21** **40**	**This work**
NiSA-N-NPGC	O-Ni-N$_4$	0.1 M KHCO$_3$	0.51 wt%	−0.76	97.2%	26.2	*ACS Nano* 2022, **16**, 2110.
Ni-N$_4$-O/C	O-Ni-N$_4$	0.5M KHCO$_3$	0.37 wt%	−0.9	99.2%	23	*Angew. Chem. Int. Ed.*, 2021, **60**, 4192.
Ni-N$_3$-C	Ni-N$_3$	0.5M KHCO$_3$	0.85 wt%	−0.65	95.6%	6.64	*Angew. Chem. Int. Ed.* 2021, **60**, 7607.
NiNG-S	Ni-N$_2$-S	0.5M KHCO$_3$	-	−0.9	90%	40.3	*Angew. Chem. Int. Ed.* 2021, **60**, 23342.
Ni-SAs@FNC	Ni-N$_4$	0.5M KHCO$_3$	5.92 wt%	−0.77	97%	22	*Appl. Catal. B: Environ.* 2021, **283**, 119591.
NiSA@N-C	Ni-N$_4$	0.1 M KHCO$_3$	0.86 wt%	−0.750	96%	25.3	*Nano Energy* 2020, **77**, 105158.
Ni-CNT-CC	Ni-N$_4$	0.5 M KHCO$_3$	0.27 wt%	−0.71	99%	32.3	*Angew. Chem., Int. Ed.* 2020, **59**, 798.
Ni-N-MEGO	-	0.5 M KHCO$_3$	6.7 wt%	−0.70	92.1%	26.8	*Appl. Catal. B: Environ.* 2019, **243**, 294.
Ni SAs/NCNTs	Ni-N$_4$	0.5 M KHCO$_3$	6.63 wt%	−1.0	97%	55.38	*Appl. Catal. B: Environ.* 2019, **241**, 113.
A-Ni-NG	Ni-N$_4$	0.5 M KHCO$_3$	4.0 wt%	−0.72	97%	30.5	*Nat. Energy* 2018, **3**, 140.

NiSA-N-CNT	Ni-N$_4$	0.5 M KHCO$_3$	20.7 wt%	−0.70	91.3%	23.5	*Adv. Mater.* 2018, **30**, 1706287.
C-Zn$_1$Ni$_4$ZIF-8	-	1.0 M KHCO$_3$	5.44 wt%	−1.13	94%	44.1	*Energy Environ. Sci.* 2018, **11**, 1204.
NiSAs/N-C	Ni-N$_3$	0.5 M KHCO$_3$	1.53 wt%	−1.00	71.9%	7.53	*J. Am. Chem. Soc.* 2017, **139** 8078.
Ni-N$_4$-C	Ni-N$_4$	0.5 M KHCO$_3$	1.41 wt%	−0.81	99%	28.3	*J. Am. Chem. Soc.* 2017, **139**, 14889.
Ni-N-C	Ni-N$_4$	0.1 M KHCO$_3$	0.7 at%	−0.78	85%	10.2	*Nat. Commun.* 2017, **8**, 944.

[a]The calculation of turnover frequency (TOF) per site was based on the estimation of the numbers of Ni active sites.

Table S3 Comparison of various electrocatalysts for CO_2RR in flow cell.

Catalyst	Atomic configuration	electrolyte	Potential (V *vs* RHE)	FE_{co}	j_{co} (mA cm^{-2})	Ref
Ni SAs/ OMMNC	**O-Ni-N$_4$**	**1.0 M KOH**	**−0.6**	**99%**	**325**	**This work**
A-Ni@CMK	Ni-N$_4$	1.0 M KOH	−0.6	99.5%	247	*Adv. Energy Mater.* 2021, 2102152.
N$_3$NiPc-CNT	Ni-N$_4$	1.0 M KOH	–	100%	>200	*Energy Environ. Sci.* 2021, **14**, 1544.
Ni-N$_4$/C-NH$_2$	Ni-N$_4$	1.0 M KOH	−0.80	89%	327.8	*Energy Environ. Sci.* 2021, **14**, 2349.
Ni@NiNCM	Ni-N$_4$	1.0 M KHCO$_3$	−0.77	93.7%	100	*Angew. Chem., Int. Ed.* 2021, **60**, 11959.
CoTMAPc @CNT	Ni-N$_4$	1.0 M KOH	−0.7	95.6%	239	*Energy Environ. Sci.* 2021, **14**, 483.
NiSA/PCFM	Ni-N$_4$	0.5 M KHCO$_3$	−1.0	88%	271.39	*Nat. Commun.* 2020, **11**, 593.
NiPc-OMe-MDE	Ni-N$_4$	1.0 M KHCO$_3$	−0.61	99.5%	150	*Nat. Energy* 2020, **5**, 684.
Ni-N@ILs	Ni-N$_4$	1.0 M KHCO$_3$	−0.65	99.4%	103	*ACS Catal.* 2020, **10**, 13171.
Fe^{3+}-N-C	-	0.5 M KHCO$_3$	−0.45	90%	94	*Science* 2019, **364**, 1091.
CoPc	Co-N$_4$	1.0 M KOH	–	95%	100	*Science* 2019, **365**, 367.
Ni-NCB	-	0.1 M KHCO$_3$	2.52 (cell voltage)	99%	>100	*Joule* 2019, **3**, 265.
Ni-N-C	Ni-N$_4$	1.0 M KHCO$_3$	−0.9	>85%	>200	*Energy Environ. Sci.* 2019, **12**, 640.

Table S4 The fitted R_s and R_{ct} of Ni SAs/OMMNC and compared samples.

Sample	Ni SAs/OMMNC	Ni SAs/OMNC	Ni NPs/OMMC
R_s (Ω)	3.35	3.59	3.75
R_{ct} (Ω)	1.48	2.22	8.50

Table S5 Performance comparison of convergent paired electrosynthesis from CO_2 to DMC and direct electrosynthesis from CO to DMC.

Catalyst	Electrosynthesis method	Current density (mA cm^{-2})	FE	Ref
Ni SAs/ OMMNC	**convergent paired electrosynthesis from CO$_2$**	**12**	**80%**	**This work**
Pd-B(iii)	electrosynthesis from CO	4	83%	*Nat. Commun.* 2019, **10**, 4807.
Copper carbonyl	electrosynthesis from CO	3	6%	*ACS Catal.* 2018, **9**, *859.*
Au/carbon	electrosynthesis from CO	11	35%	*J. Phys. Chem. B* 2005, **109**, 9140.
HAuCl$_4$/AC	electrosynthesis from CO	2.4	5.1%	*J. Am. Chem. Soc.* 2004, **126**, *5346.*
Pd/VGCF	electrosynthesis from CO	12	67%	*J. Catal.* 2004, **221**, 110.
PdCl$_2$/graphite	electrosynthesis from CO	5	60%	*Chem. Lett.* 2002, **31**, 448.
CuCl$_2$/graphite	electrosynthesis from CO	4.6	14.5%	*J. Electrochem. Soc.* 1995, **142**, 130.